Impact of operational parameters on turbidity generation in cutter suction dredging: Insights from a numerical model and sensitivity analysis

Mahgoub, Mosaab; Keetels, G.H.; Alhaddad, Said

DOI
10.1016/j.apor.2024.104312

Publication date
2025

Document Version
Final published version

Published in
Applied Ocean Research

Citation (APA)
Mahgoub, M., Keetels, G. H., & Alhaddad, S. (2025). Impact of operational parameters on turbidity generation in cutter suction dredging: Insights from a numerical model and sensitivity analysis. *Applied Ocean Research*, *154*, Article 104312. https://doi.org/10.1016/j.apor.2024.104312

Applied Ocean Research 154 (2025) 104312

Contents lists available at ScienceDirect

Applied Ocean Research

journal homepage: www.elsevier.com/locate/apor

Research paper

Impact of operational parameters on turbidity generation in cutter suction dredging: Insights from a numerical model and sensitivity analysis

Mosaab Mahgoub *, G.H. Keetels, Said Alhaddad

Section of Offshore and Dredging Engineering, Faculty of Mechanical Engineering, Delft University of Technology, Mekelweg 2, 2628 CD Delft, The Netherlands

ARTICLE INFO

Keywords:
Cutter suction dredger
Turbidity currents
Sediment plumes
Environmental impact assessment
Breaching
Sediment resuspension

ABSTRACT

The cutter suction dredger (CSD) is one of the main vessels utilized in the dredging industry. The dynamic actions related to its rotating cutter head are the main trigger for sediment release and turbidity generation by this vessel. The ability to predict the evolution of this turbidity and suspended sediment concentrations is imperative for effective environmental management. This predictive capability allows ecologists to estimate potential damage, enabling environmental managers to propose appropriate mitigation measures. In this study, we conducted a qualitative numerical assessment of the characteristics of turbidity currents generated as a result of cutter suction dredging of densely-packed sand. To this end, we developed a one-dimensional physics-based model, providing the order of magnitude of sediment fluxes and concentration levels. In addition, a quantitative sensitivity analysis is performed to unravel the relative influence of key operational parameters on the generated turbidity currents. The results of this research reveal that breaching (dilative underwater slope failure) is a major source of sediment release by CSDs and should be incorporated in the source-term estimation. It is also found that the cut ratio is the most influential operational parameter on the generated turbidity.

1. Introduction

Dredging is the process of excavating, transporting, and reallocating bed materials of a water body to another place. Such a process is necessary for different engineering applications, for instance, the construction and maintenance of harbors, navigational pathways, and flood defences. During dredging, sediment release and turbidity generation are unavoidable (Alhaddad and Elerian, 2024a) and can be triggered during one or more of the aforementioned stages of dredging (EPA, 2021). Dredging-induced turbidity poses a serious threat to the aquatic environment. Turbidity-related light reduction and its repercussions of reducing the oxygen release and the growth of aquatic flora and fauna, and the smothering of sensitive habitats like coral reefs are examples of the potential impacts of such a threat (Erftemeijer and Robin Lewis, 2006; PIANC, 2010; Erftemeijer et al., 2012; Jones et al., 2019). In the case of dredging contaminated soils (remedial dredging), another possible dangerous impact is the release and propagation of the contaminants attached to the sediment particles of the triggered sediment-laden flows (Becker et al., 2015).

To anticipate the potential environmental impacts of dredging-induced turbidity, an environmental impact assessment (EIA) is usually carried out for each dredging project (Sun et al., 2020). EIA includes far-field modelling of dredging-induced turbidity to predict its spatial and temporal evolution. Based on these far-field predictions, an ecological assessment is performed to estimate the potential damage of each environmental receptor within the concerned habitat (Erftemeijer et al., 2012) (see Fig. 1). In the far field, the propagation of dredging-induced turbidity is governed by the oceanographic environmental conditions, i.e., tidal currents, wind, and waves (Tuinhof, 2014; Shao et al., 2015). The key input to far-field models is the source-term, which is an approximation of the rate of sediment release (flux) by the dredging vessel to the far field (see Fig. 1). Accurate quantification of the source-term is essential for a realistic prediction of dredging-induced turbidity propagation and a reasonable EIA. Any uncertainty in the source-term prediction will propagate through the whole EIA process and may result in misestimated stresses (concentration levels) and environmental impacts. The source-term (quantity and distribution) depends on the used dredging vessel and its operational parameters, and the in-situ soil properties (De Wit, 2015).

CSD is the second main dredging vessel dominating the dredging industry after the trailing suction hopper dredger (TSHD). CSD has been used for both capital and maintenance dredging since the end of the 19th century (Henriksen, 2009; Mills and Kemps, 2016). The main advantage of the cutter suction dredging technique is its applicability for a broad range of soil bed formations ranging from

* Corresponding author.
E-mail addresses: M.A.A.Mahgoub@tudelft.nl (M. Mahgoub), G.H.Keetels@tudelft.nl (G.H. Keetels), S.M.S.Alhaddad@tudelft.nl (S. Alhaddad).

https://doi.org/10.1016/j.apor.2024.104312
Received 19 June 2024; Received in revised form 10 October 2024; Accepted 4 November 2024
Available online 21 November 2024

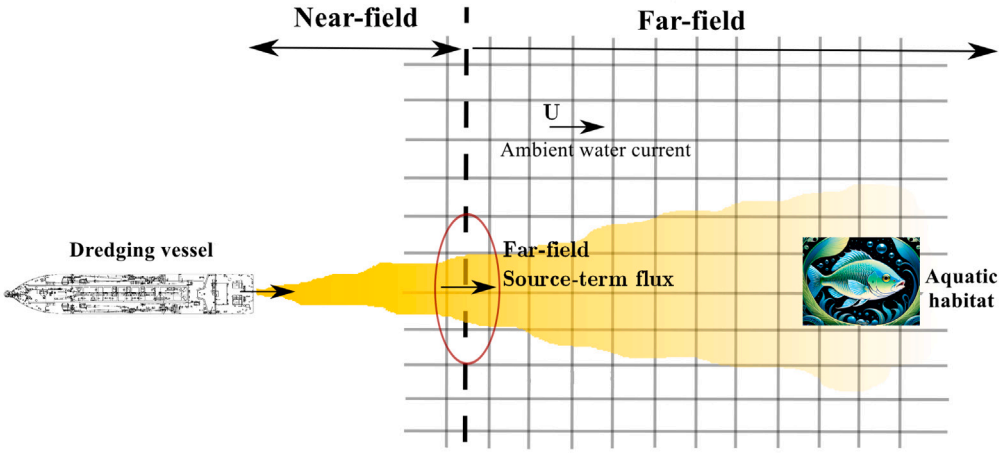

Fig. 1. Sketch of dredging-induced turbidity propagation, and the location of the source-term input (Tuinhof, 2014).

soft clay to hard rock (Mills and Kemps, 2016). In addition, CSD is distinguished by its accurate dredging profiles compared to the other dredging vessels (Den Burger, 2003; Vlasblom, 2005). CSD is mainly used for dredging bed formations that require mechanical actions to disintegrate the soil, which is mainly conducted by the cutter head (see Fig. 2(b)). Moreover, CSD is utilized for unconsolidated and non-cohesive soils (Mills and Kemps, 2016).

During dredging, sediment release is inevitable. The cutter head actions are the main trigger of sediment release and turbidity generation during cutter suction dredging. The near-field environment is complex and contains dynamic interactions: cutter-head-soil interaction, cutter-head-mixture interaction, and different sediment resuspension mechanisms. However, the common approaches followed in the dredging industry for estimating the rate of sediment release (source-term) by CSD are empirical and do not reflect these dynamics. Additionally, there is no methodology available in the literature for source-term estimation in the case of cutter suction dredging of densely-packed sand. This case is more critical, as an additional major resuspension comes into play, referred to as breaching, which is accompanied by the generation of turbidity currents (Alhaddad et al., 2020b, 2024b).

This study aims to address key limitations in existing models of turbidity currents generated by CSDs. Current empirical models are site and equipment-specific and do not consider the breaching mechanism. Additionally, the interaction between the cutter head and turbidity currents has not been previously explored. To overcome these gaps, we develop a computationally efficient, physics-based model that accounts for mixing and breaching, extending the 4-equation model by including sediment and water entrainment external sources. We also perform a global sensitivity analysis to quantify the influence of CSD operational parameters on turbidity current dynamics, the first of its kind in this context. The model's efficiency makes this analysis feasible, which would have been computationally infeasible with 3D CFD models. This allows us to identify the most influential parameter, offering valuable insights for optimizing CSD operations. Our methodology bridges the gap between empirical limitations and the need for a robust, physically-based model, advancing both scientific understanding and practical application.

This paper is structured as follows. Section 2 outlines the working method and components of CSDs. Section 3 builds on this by first explaining how sediment is released by CSDs during these operations and identifying which components are involved. Then, it provides a detailed explanation of the different resuspension mechanisms encountered during cutter suction dredging of densely-packed sand and highlights the limitations of the available source-term estimation methods in the literature. Section 4 describes the numerical assessment methodology followed in this paper, providing a detailed description of the adopted models. Section 5 provides a background on the sensitivity analysis method implemented in this study and the statistical indices used for sensitivity quantification. Section 6 presents the results of this study and the discussion. In the final section, a conclusion is formulated, and an outlook is introduced.

2. Working method of CSD

The main components of a CSD, as shown in Fig. 2(a), are the cutter head, the ladder, the suction pipe, the dredge pump, the discharge pipe, and the spud system (working spud, auxiliary spud, and spud carriage). The cutter head is the most crucial CSD component since dredging production and also sediment release heavily depend on it (Vlasblom, 2005). The cutter head is responsible for loosening the soil, creating a soil–water mixture, and guiding the mixture to the suction mouth (Den Burger, 2003). The cutter head consists of some blades, usually five to eight (Henriksen, 2009). On top of these blades, a number of cutting elements are attached through adapters, and the blades are connected together through the back ring and the hub (see Fig. 2(b)).

For the operation of CSD, a repetitive stationary swinging-stepping approach is followed with the help of the spud system, anchors, and wires (see Fig. 3). The working spud is always anchored in the bed while dredging. By slacking and pulling the side anchor wires, the CSD swings back and forth with a circular movement around the working spud. Once a swing is completed, the CSD steps forward with the help of the spud carriage and starts to swing back in the reverse direction. The swinging and stepping are repeated until the end of the spud carriage stroke is reached. Then, the auxiliary spud is lowered, and the working spud is lifted and moved to the beginning of the spud carriage stroke. Following that, the working spud is lowered, the auxiliary spud is lifted, and the whole cycle is repeated. The design of the cutter head (the orientation of the cutting blades and teeth, see Fig. 2(b)) allows only for one rotation direction, which results in two types of cutting according to the swinging direction; over-cutting and under-cutting. Over-cutting happens when the direction of swinging is the same as the cutter head rotation, while, under-cutting happens when the direction of swinging is opposite to the direction of the cutter head rotation.

The working method of the CSD, particularly the cutter head's rotation and the swinging-stepping process, directly influences turbidity generation. As the cutter head dislodges soil and mixes it with water, sediment release occurs not only through the cutting process but also due to the complex hydrodynamic interactions generated around the dredger. These interactions, along with the movement of the ladder and spud system, contribute to both sediment spillage and resuspension in the surrounding water column. Understanding the mechanisms

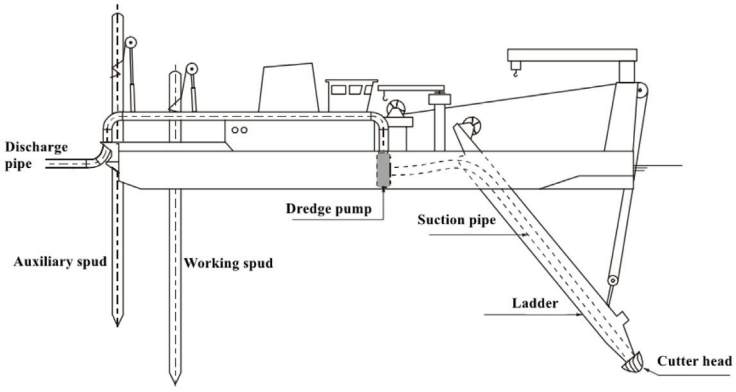

(a) Sketch of a cutter suction dredger (Vlasblom, 2005)

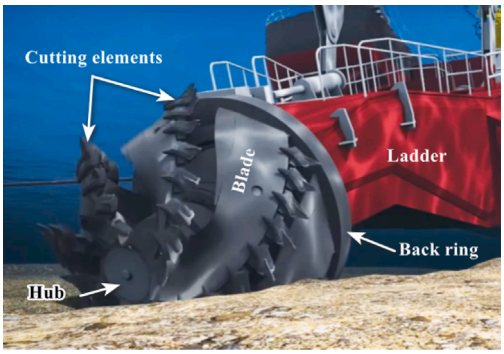

(b) The main components of cutter head (Niewboer, 2022)

Fig. 2. Main components of cutter suction dredgers.

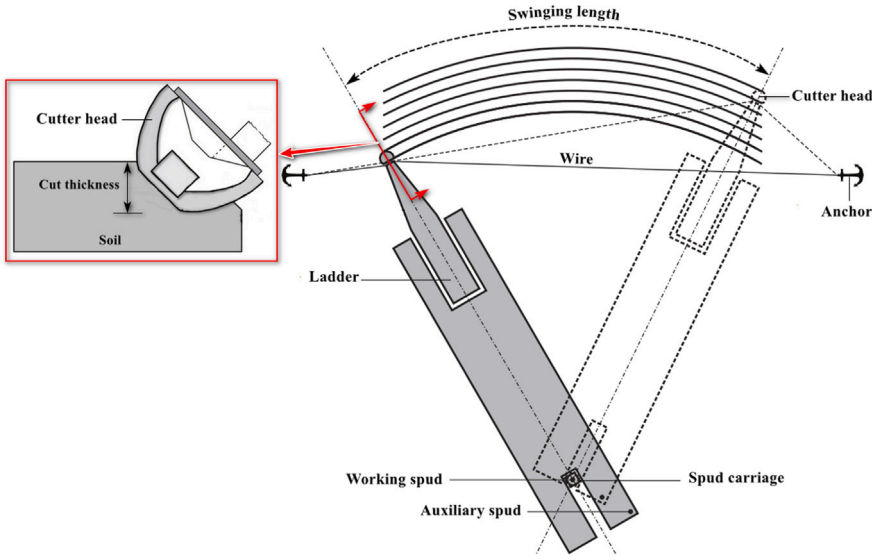

Fig. 3. Sketch illustrating the working method of cutter suction dredger (adapted from Niewboer (2022)).

behind sediment release is crucial, as they affect both the efficiency of the dredging operation and the environmental impact. The following section explores the various processes and resuspension mechanisms responsible for sediment resuspension during cutter suction dredging.

3. Sediment release and resuspension mechanisms

Sediment resuspension can occur through different processes during cutter suction dredging. For instance, in shallow dredging sites, using large CSDs with drafts close to the bed or swinging the vessel at high speed can create a turbulent flow field around the vessel and cause sediment resuspension. The ladder movement can also generate turbidity when the ladder angle is small; dragging the ladder over the bed will cause turbidity (Henriksen, 2009; HR Wallingford, 2003). Also, the movement of the spud system, anchors, and wires can release sediment from the bed (Becker, 2011). In addition, sediment plumes can occur during the transport of the dredged mixture, e.g., from overtopping while loading the mixture onto barges or from an accidental leakage from the discharge pipeline (HR Wallingford, 2003). However, the actions and processes related to the rotating cutter head are the main triggers of sediment resuspension and turbidity generation by CSD (Hayes, 1986; Henriksen, 2009; HR Wallingford, 2003). While dredging, there are some sediment losses, as not all sediment particles dislodged by the cutter head are transported through the suction pipe. This represents a concern from a production point of view, as well as an environmental point of view. From a production point of view, sediment loss is commonly known as spillage for which there are two main types: cutting spillage, and mixing spillage (Den Burger, 2003; Niewboer, 2022).

The environmental concern is related to the fines that are released to the water column, as the large particles settle fast while the fines can be kept suspended in the water column for long periods and generate turbidity flows (Becker et al., 2015). There are different mechanisms related to the cutter head with which the sediment particles can be brought into suspension. According to Hayes (1986) and Collins (1995), the main sediment resuspension mechanisms are the mechanical pickup mechanism, the wash-off mechanism, the hydrodynamic pickup mechanism, and the sloughing mass failure mechanism. The mechanical pickup mechanism is the throw of sediment particles from the cutting bank due to the centrifugal force exerted by the blades and teeth of the rotating cutter head on the sediment particles just dislodged from the cutting bank before entering the cutter head, in addition to the scattering effect of the turbulent flow field around the rotating cutter head. This mechanism is related to the cutting spillage. The wash-off mechanism is the removal of soil particles stuck to the blades and teeth of the cutter head by the turbulent flow field resulting from the cutter head rotation and ladder swinging (more significant in the case of cutter suction dredging of soils with adhesive characteristics).

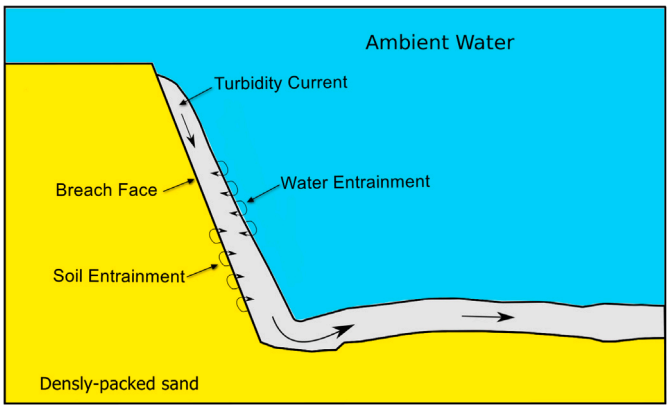

Fig. 4. Sketch of the breaching process and the associated turbidity current (Alhaddad et al., 2021).

The hydrodynamic pickup mechanism is the sediment pick up and bed erosion by the turbulent flow field around the rotating cutter head and the swinging ladder. The sloughing mechanism is the shear failure of soil mass due to the near-vertical cutting face created by the cutter head after dislodging and sucking sediment particles during each swing. The probability of such mass failure increases for less cohesive less compacted bed formations, it also increases with increasing the cutting thickness. Another cause of sloughing is the common buried-cutting technique followed by the operators to disintegrate a big sediment layer with a depth higher than the cutter diameter with only one swing (Hayes, 1986).

An additional mechanism that is highly related to the cutter head rotational speed and suction discharge is the mixing resuspension mechanism. Mixing resuspension happens due to the pumping effect of the cutter head. During the seventies of the last century, many experimental tests were carried out within the Dutch dredging industry on the cutting and mixing processes of the cutter head (Den Burger, 2003). One of the important findings was that the cutter head acts like two successive pumps: a pump with an inward flow near the nose of the cutter head and a pump with an outward flow near the back ring. The outward flow near the back ring is responsible for the mixing resuspension. The outward flow rate depends on the ratio between the rotational speed and the suction speed (Den Burger, 2003; Niewboer, 2022).

Breaching is another sediment resuspension mechanism that can be encountered in the dredging of densely-packed sandy soils, for which CSDs are commonly used. Densely-packed sand is characterized by its dilative behaviour under shear causing negative pore water pressure. This negative pressure increases the effective stress and holds the soil particles together preventing the soil mass failure. Instead, the sand particles are individually disintegrated particle by particle from the slope surface and the pore pressure is gradually dissipated (Alhaddad et al., 2023). Thus, breaching is characterized by its gradual retrogressive failure (Alhaddad et al., 2020c) (see Fig. 4).

The source-term depends on the near-field complex dynamics around the cutter head and the different resuspension mechanisms (see Fig. 5). Becker et al. (2015) summarized the common procedures followed in the dredging industry for source-term estimation for the different dredging vessels. For CSD, an empirical very simplified approach is using a percentage of the fines in the sediment that will be dredged and distributing them in time and space along the working procedure.

Another approach for source-term estimation is using one of the empirical models developed using regression analysis for the data collected during the field measurement campaigns carried out by the US Army Crop of Engineers (USACE) during the 80th of the last century. For instance, the Calumet Harbor, James River, Savannah River, New Bedford, and Lavaca Bay field measurement campaigns. This includes the models of Hayes (1986), Crockett (1993), Collins (1995), Hayes et al. (2000) and Hayes and Wu (2001). These models empirically relate the sediment release of CSD to some of its operational parameters: suction velocity, rotational speed, swinging speed, cutter diameter, and cut ratio. However, these models are site and equipment-specific and their applicability is limited to the range of operational parameters and site conditions of the data on which they were trained and validated (Hayes et al., 2000).

The common practice in the dredging industry for evaluating CSD-induced turbidity considers that the near-field turbidity triggered by the cutter head is released as a passive plume that is dispersed in the far field by the ambient water current (Hayes, 1986; Crockett, 1993; Henriksen, 2009). This assumption is not valid for the case of cutter suction dredging of densely-packed sand, especially with relatively large cutting ratios where more energetic turbidity currents are generated (see Fig. 5(e)). In this respect, it is worth mentioning that the aforementioned source-term estimation methods did not consider breaching which can be a major resuspension mechanism (see Fig. 5(c)).

4. Numerical assessment of turbidity currents

The methodology implemented in this research consists of two main parts; developing a physics-based model and performing a quantitative sensitivity analysis. The purpose of the model is to replicate and estimate the dynamics of the turbidity currents generated during cutter suction dredging of densely-packed sandy soils. Different operational scenarios are simulated to explore the impact of the main CSD operational parameters on the generated turbidity current dynamics. These parameters include the cutter head rotational speed, the ladder swinging speed, the suction discharge, and the cut ratio, i.e., the ratio of the cut thickness to the cutter head diameter. A quantitative global sensitivity analysis (GSA) approach is adopted to evaluate the degree of influence of each of these operational parameters on the CSD turbidity currents dynamics. Based on the GSA results, the most influential parameter is identified.

The developed model considers two resuspension mechanisms: the breaching mechanism, and the mixing mechanism. For model development, the turbidity current model of Parker et al. (1986), specifically, the model version of Alhaddad et al. (2020b), is extended to include multiple sediment fractions and external sources for water and sediment entrainment (see Eqs. (15)–(18)). Then, it is coupled with the analytical spillage model of Miedema (2019). The model of Parker et al. (1986) is used to represent the breaching resuspension from the breach face in addition to the propagation of the turbidity current downstream of the breach face. The model of Miedema (2019) is used to estimate the sediment-water mixture outward flow of the cutter head.

4.1. Domain and coupling method

The considered domain is a 1-D domain with a vertical breach face and a horizontal downstream part (see Fig. 6). For the breach face, the 3-equation model is implemented (Eqs. (15)–(17)), while for the downstream part, a fourth Eq. (18) is needed to take into account the turbulent kinetic energy losses due to stratification of the net-depositional flow regime. At the vertical breach face, the flow regime is erosive and fully turbulent (Eke et al., 2011).

To consider the mixing resuspension, i.e., the water and sediment external sources of the outward cutter head mixture flow, the model of Miedema (2019) is implemented (see Fig. 7). These calculated sources are averaged along the swinging path (see Fig. 6a) and distributed along the contact length of the cutter head with the breach face. Subsequently, they are used as external sources for sediment and water entrainment in the model of Parker et al. (1986). The mathematical equations are solved numerically on a discretized 1-D grid with stream-wise coordinates.

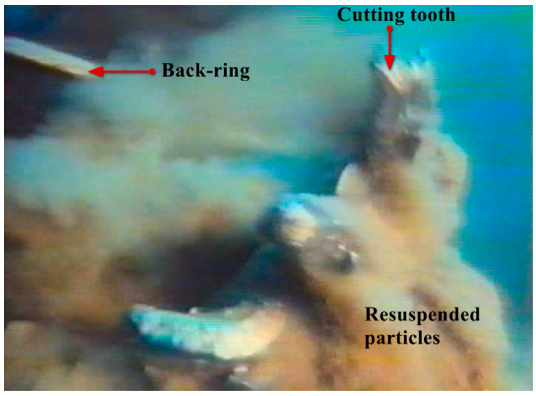

(a) Mechanical resuspension mechanism

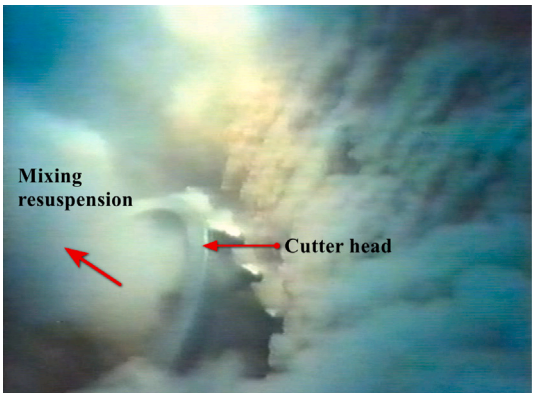

(b) Mixing resuspension mechanism

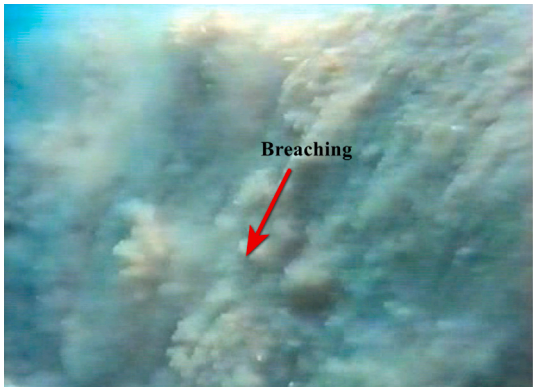

(c) Breaching resuspension mechanism

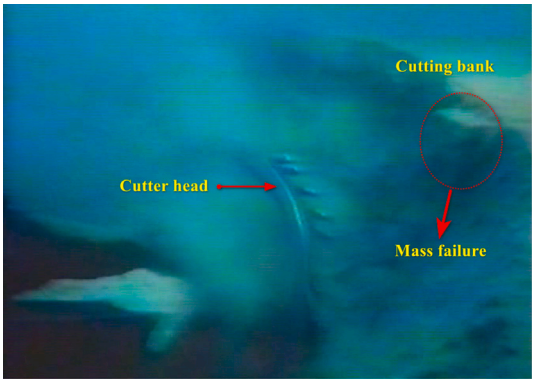

(d) Sloughing mass failure

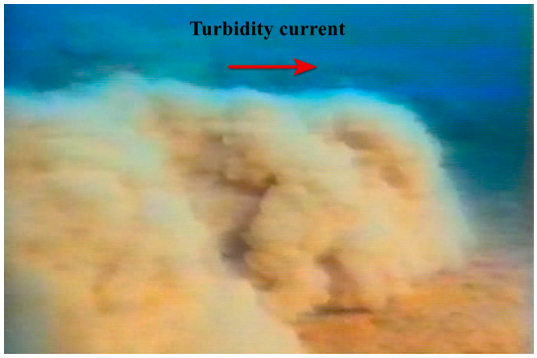

(e) CSD-induced turbidity propagating as a turbidity current

Fig. 5. Snapshots of an underwater video recorded by Jacques-Yves Cousteau for cutter suction dredging of densely-packed sand showing the different resuspension mechanisms related to the cutter head (a–d) and the propagation of the CSD-induced turbidity current (e).

4.2. 4-equation extended model

The layer-averaged 3-equation and 4-equation models introduced by Parker et al. (1986) are widely used to simulate turbidity currents in various applications, such as submarine canyons and breaching-generated turbidity currents. Initially, Parker proposed the 3-equation model based on the conservation of fluid mass (Eq. (1)), sediment mass (Eq. (3)), and mixture momentum (Eq. (12)). However, this model over-estimated sediment entrainment for highly erosive currents, leading to unrealistic conditions where turbulent kinetic energy (TKE) consumption exceeded production. To address this, a fourth equation for TKE conservation (Eq. (13)) was introduced, linking sediment entrainment to the TKE instead of the current velocity, making the 4-equation model more suitable for highly erosive currents, while the 3-equation model is better for depositional currents. Hu et al. (2015) challenged this, demonstrating analytically that the 3-equation model can apply to highly erosive currents without violating TKE conservation when realistic drag coefficients are used. This contradicts Parker's assertion that such currents excessively consume TKE. Eke et al. (2011) further investigated the models' applicability in breaching-generated turbidity currents, finding the 3-equation model causes over-acceleration on near-horizontal downstream slopes due to the lack of a mechanism for limiting bed erosion. Hence, they used the 4-equation model for the downstream regions, while applying the 3-equation model on steep, near-vertical slopes, where stratification is negligible. This study adopts

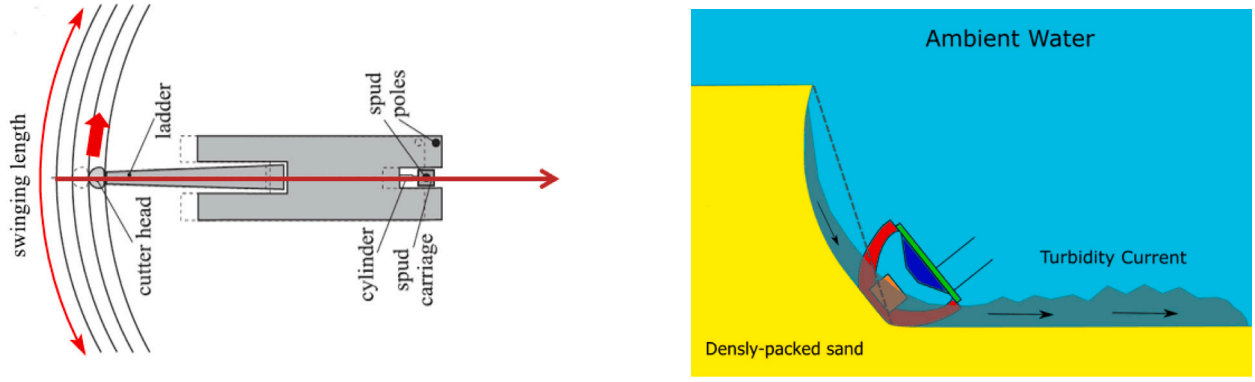

Fig. 6. Represented domain, (a) a top view of a CSD cutting and swinging along a swing path, (b) a cross-section showing the near-vertical breach generated by the cutter head and the propagation of the triggered turbidity current in the downstream.

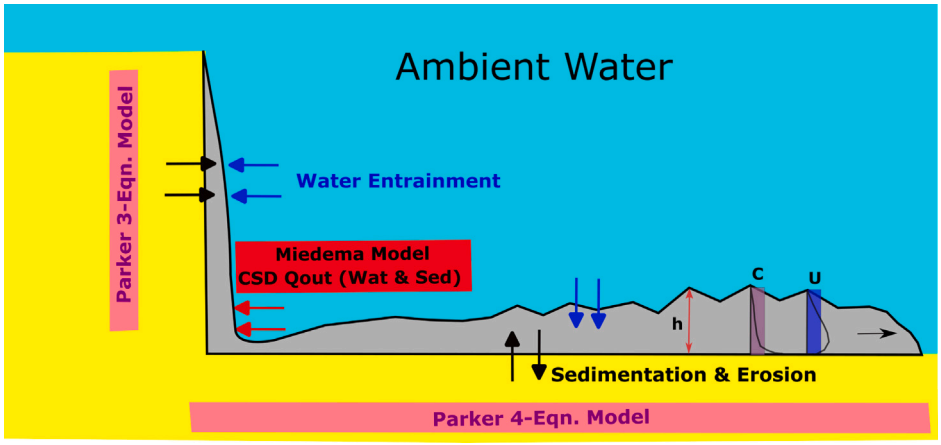

Fig. 7. Model implementation and coupling; the vertical breach face is represented by the 3-equation model of Parker et al. (1986). The external water and sediment entrainment sources (cutter head outward flow) are calculated using the model of Miedema (2019) and averaged along the swinging length (see Fig. 6). The downstream turbidity current is represented by the 4-equation model of Parker et al. (1986). h is the layer thickness, C is the layer-averaged concentration, and U is the layer-averaged velocity.

Eke's approach due to similarities with our domain and research focus on breaching.

In the 4-equation model, Eq. (1) represents the fluid mass conservation. The main source is the water entrainment at the upper interface of the turbidity current by the mixing effect resulting from the Kelvin–Helmholtz instabilities formed due to the shear stress at the interface between the stagnant clear water and the propagating soil–water mixture. Parker et al. (1987) introduced the dimensionless water entrainment coefficient (e_w) as an empirical closure (Eq. (2)) for estimating the water entrainment rate. In this study, an additional source (S_w) is added to consider the water portion of the cutter head outward flow.

$$\frac{\partial h}{\partial t} + \frac{\partial (hU)}{\partial x} = e_w U + S_w \tag{1}$$

$$e_w = \frac{0.00153}{0.0204 + Ri}, \tag{2}$$

where, h [m] is the turbidity current layer thickness, U [m/s] is the layer-averaged velocity (see Fig. 7), and $Ri = \frac{\Delta g h C}{U^2}$ [−] is Richardson number. $\Delta = \frac{\rho_s - \rho_w}{\rho_w}$ [−] is the relative submerged density of the in-situ soil particles, in which ρ_s [kg/m^3] is sediment particle density, and ρ_w [kg/m^3] is water density.

For sediment mass conservation (Eq. (3)), the main governing processes are sediment entrainment and sediment deposition (the first and second terms in the RHS of Eq. (3) respectively). Both processes depend on the sediment particle size (Parker et al., 1986; Alhaddad et al., 2020b). Additionally, in this study, an external source (S_s) is added for considering sediment entrainment by the cutter head.

$$\frac{\partial (hC_i)}{\partial t} + \frac{\partial (hUC_i)}{\partial x} = b_i w_{s,i} E_{s,i} - w_{s,i} C_{b,i} + b_i S_s, \tag{3}$$

where, the subscript i represents a particle size index, for each size, b_i [−] is the fraction of this particle size within the bed soil, C_i [−] is the layer-averaged concentration of this particle size inside the turbidity current, $w_{s,i}$ [m/s] is the hindered settling velocity, and $E_{s,i}$ [−] is the dimensionless sediment entrainment rate. $C_{b,i}$ [−] is the volumetric near-bed concentration and is empirically related to the layer-averaged concentration through the formula: $C_{b,i} = r_{0,i} C_i$ (Fukushima et al., 1985). Parker (1982) introduced an empirical closure for the ratio ($r_{0,i}$) between the near-bed concentration and the layer-averaged concentration by representing the vertical distribution of the turbidity current concentration using the Rousean expression. This empirical closure reads: $r_{0,i} = 1 + 31.5(u_*/w_{s,i})^{-1.46}$, in which u_* [m/s] is the bed shear velocity. For sediment deposition estimation, the formula of Richardson and Zaki (1954) is used as an empirical closure to the hindered settling velocity, which reads: $w_{s,i} = w_{0,i}\left(1 - C_{b,i}\right)^{n_i}$. $w_{0,i}$ [m/s] is the terminal settling velocity of the ith particle size and is calculated using the empirical closure formula of Ferguson and Church (2004) (Eq. (4)), and the power n_i [−] is calculated using the formula of Richardson and Zaki (1954) (Eq. (5)).

$$w_{0,i} = \frac{\Delta g \left(D_i\right)^2}{B_1\, \upsilon + \sqrt{0.75\, B_2\, \Delta g \left(D_i\right)^3}}, \tag{4}$$

$$n_i = \begin{cases} 4.65 & Re_{p,i} < 0.2 \\ 4.35(Re_{p,i})^{-0.03} & 0.2 < Re_{p,i} < 1 \\ 4.45(Re_{p,i})^{-0.1} & 1.0 < Re_{p,i} < 500 \\ 2.39 & 500 < Re_{p,i} \end{cases}, \quad Re_{p,i} = \frac{w_{0,i} D_i}{\nu}, \tag{5}$$

where, D_i [m] is the mean diameter of the ith particle size, B_1 [−] is a constant related to the shape of the sediment particle and ranges between 18 and 24, and B_2 [−] is an approximate value for the drag coefficient of the sediment particle and ranges between 1.0 and 1.2 for natural grains (Ferguson and Church, 2004). $Re_{p,i}$ [−] is a particle Reynolds number related to the terminal settling velocity of ith particle size, ν [m^2/s] is the kinematic viscosity of the sediment-water mixture and is assumed to be equal to the kinematic viscosity of clear water (10^{-6} m^2/s) for low-concentration mixtures (Groenenberg et al., 2009).

To estimate the sediment entrainment along the vertical breach face, the sediment entrainment coefficient, Es_i [−], is calculated using the formula put forward by (Alhaddad et al., 2020a):

$$Es_i = \frac{(1-n_0)\, u_{s,i}}{w_{s,i}} \left(\frac{v_{e,g}}{2u_{s,i}} + \sqrt{\left(\frac{v_{e,g}}{2u_{s,i}}\right) + \frac{\phi_{p,f,i} \Delta k_l f}{u_{s,i} \delta n}} \right), \tag{6}$$

where, n_0 [−] is the undisturbed bed porosity, $w_{s,i}$ [−] is the hindered settling velocity of the ith particle size, $u_{s,i} = \sqrt{\Delta g D_i}$ [m/s] is the Shields velocity for particles with the diameter D_i, $\delta n = \frac{n_l - n_0}{1-n_l}$ [−] is the relative change of the porosity of the in-situ bed soil, n_l [−] is the maximum porosity of the in-situ bed soil, k_l [m/s] is the loose-state permeability of the in-situ bed soil, $f = (\sin(\alpha_s - \phi))^{0.55}$ [−], $v_{e,g}$ [m/s] is the pure breaching bed erosion velocity, also known as the wall velocity, and is calculated using the formula of Breusers (1977) which reads:

$$v_{e,g} = -\Delta k_l \frac{\sin(\phi - \alpha_s)}{\sin\phi} \frac{(1-n_0)}{\delta n}, \tag{7}$$

in which, ϕ [°] is the internal friction angle of the bed soil, α_s [°] is the bed slope. $\phi_{p,f,i}$ [−] is the dimensionless flow-induced sediment pickup rate calculated using the formula of Alhaddad et al. (2020a) which reads:

$$\phi_{p,f,i} = 0.00052 f_{r,i} (D_{*,i})^{0.3} \left(\frac{\theta_i - f_{cr,i}\theta_{cr,i}}{f_{cr,i}\theta_{cr,i}} \right)^{1.5}, \tag{8}$$

where, $f_{r,i}$ [−] is a reduction factor for the effect of near-bed concentration (Alhaddad et al., 2020a), $D_{*,i}$ [−] is a dimensionless diameter of the ith particle size, θ_i [−] is the Shields parameter of the ith particle size, $\theta_{cr,i}$ [−] is the critical Shields parameter of the ith particle size and is calculated using the formula of Brownlie (1982). $f_{cr,i}$ [−] is an amplification factor for the critical shear stress. $f_{r,i}$, $D_{*,i}$, θ_i, and $f_{cr,i}$ are calculated based on the work of Alhaddad et al. (2020b) using the following formulas:

$$f_{r,i} = \frac{1 - n_0 - C_{b,i}}{1 - n_0}, \quad D_{*,i} = D_i \sqrt[3]{\frac{\Delta g}{\nu^2}}, \quad \theta_i = \frac{u_*^2}{\Delta g D_i}, \quad f_{cr,i} = 1 + (\sin(\phi - \alpha_s))^2, \tag{9}$$

in which, u_* [m/s] is the bed shear velocity.

Along the horizontal downstream part, sediment particles are loose and sediment entrainment is only flow-induced with no dilatancy effect, thus, the sediment entrainment coefficient, Es_i [−], is calculated using the sediment entertainment formula of Garcia and Parker (1993) developed for turbidity currents and reads:

$$E_{s,i} = \frac{1.38 \cdot 10^{-7} Z_i^5}{1 + (4.6 \cdot 10^{-7} Z_i^5)}, \quad Z_i = \begin{cases} \left(\frac{u_*}{w_{s,i}}\right)(Re^*_{p,i})^{0.6} & Re^*_{p,i} > 3.5 \\ 0.586\left(\frac{u_*}{w_{s,i}}\right)(Re^*_{p,i})^{1.23} & 1 < Re^*_{p,i} < 3, \end{cases} \tag{10}$$

where, $Re^*_{p,i}$ [−] is the particle Reynolds number of the ith particle size based on the Shields velocity ($u_{s,i}$) and is calculated using the following formula:

$$Re^*_{p,i} = D_i \frac{\sqrt{\Delta g D_i}}{\nu}, \tag{11}$$

The momentum conservation principle is applied to the soil–water mixture. The sources include the pressure gradient due to density gradient, and gravity, while the sink is the bed friction (see Eq. (12)).

$$\frac{\partial(hU)}{\partial t} + \frac{\partial(hU^2)}{\partial x} = -\frac{1}{2}\Delta g \frac{\partial(h^2 C_t)}{\partial s} + \Delta g h C_t \sin\alpha_s - u_*^2, \tag{12}$$

where, C_t [−] is the total concentration of the sediment particles, $C_t = \sum C_i$. For u_*, there are two empirical closures: $u_* = \sqrt{C_f U^2}$ for the 3-equation model, and $u_* = \sqrt{\alpha_k K}$ for the 4-equation model. K [m^2/s^2] is the layer-averaged turbulent kinetic energy, C_f [−] is the bed friction coefficient for turbidity currents. α_k [−] is a proportionality constant that relates the bed shear velocity of the turbidity current to its turbulent kinetic energy and ranges between 0.05 and 0.5 (Parker et al., 1986; Kostic and Parker, 2006).

For the turbulent kinetic energy, the source is the turbulence production at the upper and lower interfaces of the turbidity current, while the sinks include turbulent kinetic energy dissipation due to viscosity and the energy consumption against stratification (Parker et al., 1986). The equation of turbulent kinetic energy conservation reads:

$$\frac{\partial(hK)}{\partial t} + \frac{\partial(hKU)}{\partial x} = u_*^2 U + \frac{e_w U^3}{2} - \epsilon_0 h - \frac{\Delta g h}{2} \sum \left(2 w_{s,i} C_i + e_w U C_i + w_{s,i}(b_i E_{s,i} - C_{b,i})\right) \tag{13}$$

where, ϵ_0 [m^2/s^3] is the mean rate of turbulent kinetic energy dissipation and is calculated based on the work of Parker et al. (1986) using the following equations:

$$\epsilon_0 = \beta_0 \frac{K^{1.5}}{h}, \quad \beta_0 = \frac{\frac{1}{2} e_w \left(1 - Ri - 2\frac{C_{f*}}{\alpha_k}\right) + C_{f*}}{\left(\frac{C_{f*}}{\alpha_k}\right)^{1.5}}, \tag{14}$$

in which, C_{f*} is the bed friction coefficient at the equilibrium state of the turbidity current (erosion = deposition) (Parker et al., 1986).

Assuming a steady state and doing some rearrangements, the partial differential equations (PDEs) (Eqs. (1), (3), (12), and (13)) can be transformed to a set of coupled ordinary differential equations (ODEs) (Eqs. (15)–(17)). These ODEs represent the 4-equation extended model of this research. This model is an updated version of the model applied by Alhaddad et al. (2020b) to a typical case of a breaching slope.

$$\frac{dh}{dx} = \frac{-Ri \sin\alpha_s + \left(e_w + \frac{S_w}{U}\right)\left(2 - \frac{Ri}{2}\right) + \left(\frac{u_*}{U}\right)^2 + \frac{Ri}{2U\sum C_i} \sum \left(w_{s,i}(b_i E_{s,i} - C_{b,i}) + b_i S_s\right)}{1 - Ri} \tag{15}$$

$$\frac{dU}{dx} = \frac{U}{h} \times \frac{Ri \sin\alpha_s - \left(e_w + \frac{S_w}{U}\right)\left(1 + \frac{Ri}{2}\right) - \left(\frac{u_*}{U}\right)^2 - \frac{Ri}{2U\sum C_i} \sum \left(w_{s,i}(b_i E_{s,i} - C_{b,i}) + b_i S_s\right)}{1 - Ri} \tag{16}$$

$$\frac{d\left(hUC_i\right)}{dx} = w_{s,i}(b_i E_{s,i} - C_{b,i}) + b_i S_s \tag{17}$$

$$\frac{dK}{dx} = \frac{U^2}{h}\left[\left(\frac{e_w}{2}(1 - Ri)\right) + \frac{u_*^2}{U^2} - \left(e_w + \frac{S_w}{U}\right)\left(\frac{K}{U^2}\right) - \left(\epsilon_0 \frac{h}{U^3}\right)\right] - \frac{U^2}{h}\left[\left(\frac{Ri \sum b_i w_{s,i}}{U}\right) + \frac{Ri}{2U\sum C_i} \sum \left(w_{s,i}(b_i E_{s,i} - C_{b,i}) + b_i S_s\right)\right], \tag{18}$$

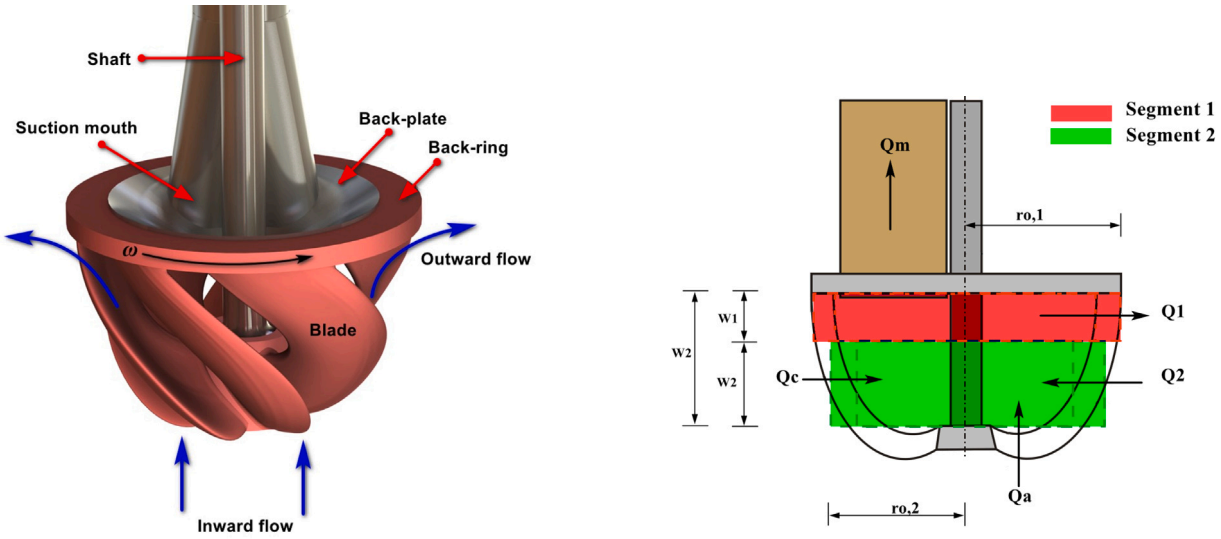

(a) Flow regime of a freely rotating cutter head (adapted from Niewboer (2022))

(b) Cutter head representation in the analytical spillage model of Miedema (adapted from Miedema (2019))

Fig. 8. The conceptual base of the analytical spillage model of Miedema (2019). ω [rad/s] is the angular velocity of the cutter head. Q_c [m^3/s] is the theoretical cutting production ($Qc = A_{cut} \times V_{swing}$). A_{cut} [m^2] is the cross-section area of the cutter head perpendicular to the swinging speed (V_{swing}) and intersected with the cutting bank. Q_1 [m^3/s] is the outward flow near the back-ring, Q_2 [m^3/s] is the inward flow near the hub. Q_m [m^3/s] is the mixture flow through the suction mouth, Q_a [m^3/s] is an axial flow. $r_{o,1}$ and $r_{o,2}$ [m] are the outer radii of Segment 1 and Segment 2 impellers. W_1 [m] is the height of Segment 1, W_2 [m] is the height of Segment 2, and W [m] is the total height of the cutter head.

Along the breach face, the 3-equation model (Eqs. (15)–(17)) is implemented, whereas the 4-equation model (Eqs. (15)–(18)) is implemented along the downstream part. In this study, C_f is taken equal to 0.027 based on calibration and validation trials using the experimental data of Alhaddad et al. (2020c). For the downstream part, C_{f*} and α_k are taken to be equal to 0.004 and 0.1, respectively.

4.3. The CSD analytical spillage model of Miedema

The CSD model of Miedema (2019) is an analytical model developed for quantifying the cutter head mixing spillage for sand and rock bed formations. The model is based on the conceptual representation of the cutter head as a centrifugal pump with two segments of different impeller sizes; a segment with an outward flow near the back-ring of the cutter head and a segment with an inward flow near the cutter head hub (see Fig. 8(b)). This conceptual representation is based on the flow characterization illustrated by Den Burger (2003) (see Fig. 8(a)). The flow is sucked through the blades contour near the hub and is accelerated towards the back-ring generating an outward flow (the pumping effect of the cutter head) (Den Burger, 2003) (See Fig. 8(a)).

The first version of the analytical spillage model (the basic model) was introduced by Miedema in 2017 based on the affinity laws of centrifugal pumps (Miedema, 2019; Niewboer, 2022). In the basic model, the cutter head geometry is simplified as a truncated cone (see Fig. 9(a)) with only considering the outer radii, the cutter head rotational speed, and the mixture discharge through the suction pipe. The cutting production is theoretically approximated based on the cut ratio and the swinging speed. This basic model was firstly implemented by Louis (2017), it is also published by Werkhoven et al. (2018). For a better representation of the cutter head geometry, Werkhoven (2019), and Miedema and Nieuwboer (2019) presented an updated version of the analytical spillage model (the advanced model) based on the Euler equation of pumps. Compared to the basic model, the advanced model provides a possibility for including a representation of the inner radii of the cutter head and the blade angles. Both the basic and advanced models showed a good agreement with the experimental data of Den Burger (2003) and Miedema (2019). For simplicity, the basic model is adopted in this research.

The affinity laws of centrifugal pumps are a set of proportionality equations used to predict the change in the pump discharge, pressure head (difference), and power as a result of changing the impeller diameter of the pump and/or the rotational speed (Karassik et al., 2008). Starting from the affinity laws of centrifugal pumps for both the discharge and pressure head (Eqs. (19)), and using proportionality coefficients, Miedema (2019) derived Eq. (20) for calculating the discharge and Eq. (21) for calculating the pressure head (difference).

$$Q_i \propto n_i\ D_i^2\ W_i \quad , \quad \Delta p_i \propto n_i^2\ D_i^2 \tag{19}$$

$$Q_i = \alpha \cdot 2 \cdot \pi \cdot r_i^2 \cdot \omega_i \cdot W_i \tag{20}$$

$$\Delta p_i = \epsilon \cdot \rho_m \cdot \omega_i^2 \cdot r_i^2, \tag{21}$$

where, Q_i [m^3/s] is the discharge of the centrifugal pump i, Δp_i [Pa] is the pressure head (difference) of the centrifugal pump, n_i [RPM] is the number of revolution per minute for the impeller of the centrifugal pump, D_i [m] is the impeller diameter, W_i [m] is the width of the impeller, α [−] is a proportionality coefficient for the discharge, ϵ [−] is a proportionality coefficient for the pressure head, ω_i [rad/s] is the angular velocity of the impeller, ρ_m [kg/m^3] is the density of the pumped fluid or mixture, r_i [m] is the radius of the impeller.

Combining Eqs. (21) and (20), Miedema (2019) expressed the discharge through the centrifugal pump as a function of the pressure head as follows:

$$Q_i = \frac{2 \cdot \pi \cdot \alpha}{\epsilon \cdot \rho_m \cdot \omega_i} \cdot \Delta p_i \cdot W_i. \tag{22}$$

To apply this equation on the two segments of the hypothetical centrifugal pump representing the cutter head, Miedema (2019) made some assumptions. It is assumed that the pressure outside the cutter head is constant, the outward flow of segment 1 (Q_1) is driven by Δp_1, the inward flow of segment 2 ($Q2$) is driven by ($\Delta p_1 - \Delta p_2$), and the mixture densities of Q_1 and Q_2 are equal to the water density (see Figs. 8(b),

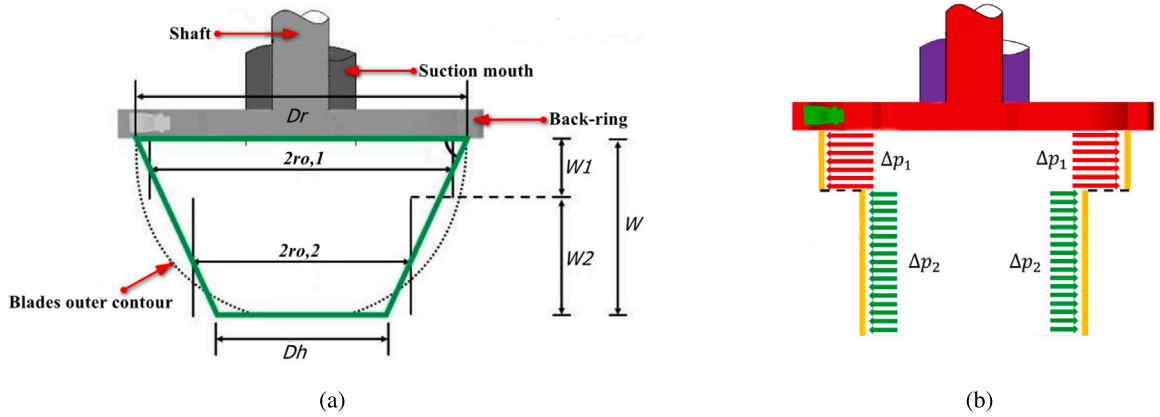

Fig. 9. Cutter head simplified geometry representation in the basic analytical model of Miedema (a), and the pressure difference generated on the blades of segment 1 (Δp_1) and segment 2 (Δp_2) of the hypothetical centrifugal pump representing the cutter head due to cutter head rotation (b). D_r is the diameter of the back-ring, D_h is the cutter head outer diameter near the hub (Werkhoven, 2019).

9(b)). Applying this, and using Eq. (22), Q_1 *and* Q_2 can be represented by the following equations:

$$\begin{aligned} Q_1 &= \frac{2\cdot\pi\cdot\alpha}{\epsilon\cdot\rho_{water}\cdot\omega}\cdot\Delta p_1\cdot W_1 \quad , \\ Q_2 &= \left(\Delta p_1-\Delta p_2\right)\cdot\frac{2\cdot\pi\cdot\alpha}{\epsilon\cdot\rho_{water}\cdot\omega}\cdot(W-W_1) \end{aligned} \tag{23}$$

Utilizing the principle of flow volume conservation for the discharges going in and out of the cutter head ($Q_c+Q_a+Q_2-Q_m-Q_1=0.0$), (see Fig. 8(b)), and applying Eqs. (23) with considering the percentage of the cutter head circumference impeded in the bank (P_c), W_1 can be calculated as follows:

$$W_1 = \frac{r_{o,1}^2-r_{o,2}^2}{2r_{o,1}^2-r_{o,2}^2}\cdot W - \frac{r_{o,1}^2}{2r_{o,1}^2-r_{o,2}^2}\cdot\frac{1}{2\pi\alpha\omega}\cdot\left(\frac{Q_m-Q_c-Q_a}{r_{o,1}^2\cdot(1-P_c)}\right). \tag{24}$$

However, Eq. (24) cannot be solved directly as $r_{o,1}$, and $r_{o,2}$ are functions of W_1 (Miedema, 2019). For the simplified geometry of the cutter head presented in Fig. 9(a), these functions are linear (Eqs. (25)). Thus, W_1 is calculated implicitly by solving Eqs. (24), (25) together through iterations starting with initial values of $r_{o,1}$ and $r_{o,2}$ equal to the radius of the back-ring and the radius near the hub respectively.

$$\begin{aligned} r_{o,1} &= \frac{D_h}{2}+\frac{(2W-W_1)\,(D_r-D_h)}{4W} \quad , \\ r_{o,2} &= \frac{D_h}{2}+\frac{(W-W_1)\,(D_r-D_h)}{4W}, \end{aligned} \tag{25}$$

having W_1 calculated, Q_1 can be estimated as follows:

$$Q_1 = 2\pi\alpha\omega\cdot W_1\cdot(1-P_c), \tag{26}$$

For calculating the spillage, Miedema (2019) assumed that the sediment concentration in the suction discharge (C_m) is the same as in the outward flow of Segment 1 (C_1), and that the inward flow (Q_1) and the axial flow (Q_a) contain clear water only. So, C_1 is calculated by applying the conservation principle for the sediment volume inside the cutter head (Eq. (27)). Then, the spillage can be estimated as the ratio of the sediment amount in the outward flow to the cutting production (Miedema, 2019). In this research, the external sources (S_w, *and* S_s) applied in the extended Parker model (Eqs. (15)–(18)) are approximated by distributing the outward mixture flow of the cutter head along the swinging length and the contact height between the cutter head and the cutting bank (Eqs. (28)).

$$Q_C(1-n_0) = Q_m C_m + Q_1 C_1 \tag{27}$$

$$S_s = \frac{Q_1\ C_1}{L_s\ h_c} \quad , \quad S_w = \frac{Q_1\ (1-C_1)}{L_s\ h_c} \tag{28}$$

where, L_s is the swinging length, and h_c is the contact height between the cutter head and the cutting bank.

Miedema (2019) calibrated the basic model against the experimental data of Den Burger (2003) for both sand and rock using the calibration parameter (α) which is dependent on the cutter head geometry and the in-situ bed material. It is worth mentioning that, although an axial flow (Q_a) is introduced in the model, it was neglected by Louis (2017), Werkhoven et al. (2018), and Miedema (2019) due to complexity as there is no available approach in the literature for quantifying it. Good agreement was found between the model spillage estimations and the experimental results of Den Burger (2003) for sand at ($\alpha = 0.162$) and for rock at ($\alpha = 0.21$) for both the prototype and scaled-down cutter head. The cutter head used in the current research is the same one utilized by Miedema (2019), thus the same calibration value for sand is adopted ($\alpha = 0.162$).

The analytical spillage model of Miedema provides a physics-based approach for quantifying the cutter head mixing spillage which is one of the main resuspension mechanics for cutter suction dredgers. However, the development of this model included some approximations and assumptions; the geometry of the cutter head is simplified as segments of centrifugal pumps with different impeller sizes assuming constant pressure outside the cutter head and an inviscid flow field (Niewboer, 2022). Also, some assumptions related to the cutter head fluxes were adopted as mentioned earlier. The main limitations of the model are its dependence on empirical factors, and not being validated due to data availability (Niewboer, 2022).

5. Sensitivity analysis

Sensitivity analysis is widely utilized in water and environmental modelling applications for calibration, uncertainty quantification, and informed decision-making (Pianosi et al., 2016). There are two main categories for sensitivity analysis: local-based approaches and global-based approaches which are known as Global Sensitivity Analysis (GSA) (Saltelli et al., 2008). Local sensitivity analysis investigates the model output changes resulting from changing the model inputs locally around a certain point within the domain of inputs, usually around a reference point or a base scenario. Such a local approach is unsuitable for non-linear models (Pianosi et al., 2016; Saltelli et al., 2019). On the other hand, in GSA, the sensitivity is quantified based on many scenarios that are sampled using an All-at-a-time (AAT) approach and distributed along the whole domain of inputs allowing for detecting higher-order sensitivities. In the AAT approach, the inputs are sampled simultaneously. This means that instead of varying one input parameter per sample while keeping the other parameters fixed, each sample is generated as a point in the multidimensional input space where all

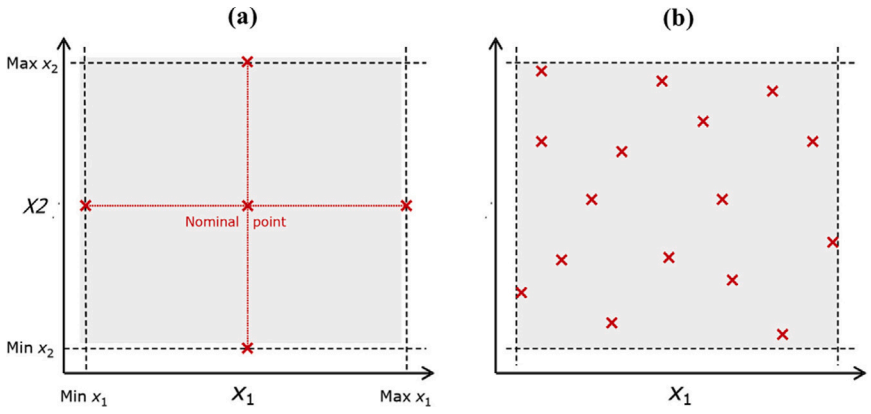

Fig. 10. Inputs domain covering for the OAT (a), and the AAT (b) sampling approaches (Saltelli et al., 2019).

parameters are allowed to vary. Compared to local sensitivity analysis, GSA is more robust for non-linear models in which the sensitivity would be different from point to point within the domain of inputs (Pianosi et al., 2016; Saltelli et al., 2019).

The most simple and common approach for local sensitivity analysis is the One-at-a-time (OAT) approach. In OAT sensitivity analysis, the significance of each model input is assessed separately by estimating the relative change of the model output resulting from relatively changing the concerned parameter from its reference value while keeping the other parameters unchanged (Saltelli et al., 2008; Iooss and Lemaître, 2015; Borgonovo and Plischke, 2016). For GSA, the method of Sobol (1990) is the most popular (Brandstäter, 2021) and is widely adopted in environmental modelling (Pianosi et al., 2016). Fig. 10 compares between the OAT sampling approach and the AAT sampling approach adopted in GSA for a case of two model inputs (X1, and X2). It can be noted that for the OAT, the model is only assessed along certain paths crossing a reference case (Nominal point) covering only a very small part of the domain of inputs (the X1-X2 domain). The uncovered parts of the inputs domain may have different model behaviours. While, in the AAT sampling, the samples are distributed along the (X1-X2) domain.

The Sobol GSA is a variance-based method developed by Sobol (1990) based on the Analysis of Variance (ANOVA) decomposition (Archer et al., 1997; Sobol, 2001). In the method of Sobol (1990), the sensitivity of the model output (Y) to each input parameter (X_i) is quantified through two main indices: the first-order sensitivity index (S_i), and the total sensitivity index (S_i^T). S_i reflects the direct contribution of the model input (X_i) to the variance of the model output (Y). It quantifies the relative reduction of the variance of (Y) that would result from keeping the input parameter X_i fixed (Saltelli et al., 2008; Brandstäter, 2021) (Eq. (29)). On the other hand, S_i^T reflects the total contribution of the input parameter (X_i) to the variance of the model output (Y) including the direct contribution and the higher order interactions of the input parameter (X_i) with the other input parameters (Saltelli et al., 2008). S_i^T quantifies the remaining relative variance of (Y) if all the input parameters except X_i ($X_{\sim i}$) are kept fixed (Saltelli et al., 2008; Brandstäter, 2021) (Eq. (30)).

$$S_i = \frac{\mathrm{Var}_{X_i}\left[E_{X_{\sim i}}[Y|X_i]\right]}{\mathrm{Var}_X[Y]} \tag{29}$$

$$S_i^T = 1 - \frac{\mathrm{Var}_{X_{\sim i}}\left[E_{X_i}[Y|X_{\sim i}]\right]}{\mathrm{Var}_X[Y]} = \frac{E_{X_{\sim i}}\left[\mathrm{Var}_{X_i}[Y|X_{\sim i}]\right]}{\mathrm{Var}_X[Y]}, \tag{30}$$

where, $E_{X_{\sim i}}[Y|X_i]$ is the conditional expectation of the model output (Y) given the input parameter X_i, $\mathrm{Var}_X[Y]$ is the unconditional total variance of (Y), $\mathrm{Var}_{X_i}[Y|X_{\sim i}]$ is the conditional variance of (Y) given the all input parameters (X) except X_i.

The main limitation of the method of Sobol (1990) is being computationally expensive; a large number of samples is needed to be evaluated by the model (thousands of samples) (Iooss and Lemaître, 2015). However, this was not a hindrance in this research, as the implemented model is computationally efficient; each run of the model takes only a few seconds. Thus, the method of Sobol (1990) is used to quantify the relative importance of each operational parameter as the local sensitivity approach is not applicable due to the non-linearity of the model developed in this research.

6. Results and discussion

To achieve the objective of this research, the developed model is numerically implemented on a 1-D discretized grid with a stream-wise coordinate system for a test case (Fig. 11). The system of ordinary differential equations ($N + 2$ for the 3-equation model), and ($N + 3$ for the 4-equation model) is solved numerically using the explicit Euler method, where N is the number of sediment fractions. Small arbitrary values are used as boundary conditions to avoid the numerical error of division by zero when having zero boundary conditions (see Figs. 12, 13). Five different boundary condition cases are tested for the layer thickness (h_0), layer-averaged velocity (U_0), and layer-averaged concentration (C_0). Case 1, representing the boundary conditions used in this study, serves as the reference. The relative increases in the boundary condition values range from 25% to 100%. For each case, the relative changes in the turbidity current results at the end of the simulated domain, specifically, layer-averaged velocity (U_L), layer-averaged concentration (C_L), and total sediment flux (q_L), are recorded. Table 1 summarizes the boundary condition values for each case (h_0, C_0, and U_0), along with the corresponding relative changes (ΔU_L, ΔC_L, and Δq_L).

From Table 1, it can be observed that the relative changes are quite small (3.5% at maximum). Moreover, the spatial distribution trends of the turbidity current characteristics remained the same across all tested boundary condition cases. This consistency aligns with the self-acceleration nature of the breaching turbidity current along the steep breach face, primarily driven by sediment entrainment from bed erosion.

The simulated test case includes an in-situ bed material of densely-packed sand assuming that a vertical breach is generated after each swing and a horizontal downstream part (see Fig. 11). The properties of the in-situ densely-packed sand are listed in Table 2. For the cutter suction dredger, the operational data of the prototype cutter head of Den Burger (2003) experiments is used as a reference case, the same data that Miedema used to calibrate his model. The geometry and operational parameters of the test case are listed in Fig. 11.

For investigating the impact of the operational parameters (rotational speed, swinging speed, suction discharge, and cut ratio) on the

Table 1
Model sensitivity to boundary conditions.

Case #	$h_0 \times 10^{-3}$ [m]	$C_0 \times 10^{-2}$ [–]	$U_0 \times 10^{-1}$ [m/s]	ΔU_L [%]	ΔC_L [%]	Δq_L [%]
1	1.00	1.00	1.00	0.0	0.0	0.0
2	1.25	1.25	1.25	−0.85	−3.2	−3.5
3	1.50	1.50	1.50	−0.77	−2.9	−3.1
4	1.75	1.75	1.75	−0.66	−2.5	−2.7
5	2.00	2.00	2.00	−0.51	−1.9	−2.1

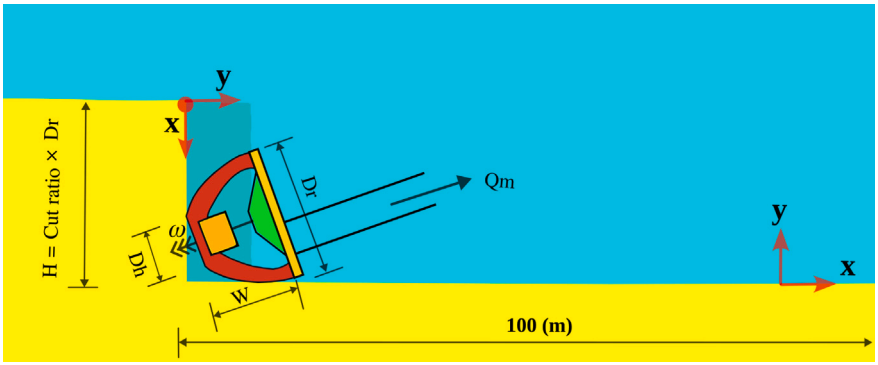

Fig. 11. Sketch of the adopted reference case, $H = Cut_{ratio} \times D_r$ is the breach height, $Cut_{ratio} = 1.0$ ($D_r = H$), $D_r = 3.12$ [m] is the diameter of the cutter head back-ring, $D_h = 2.11$ [m] is the cutter head diameter near the hub, $W = 2.5$ [m] is the cutter head height, $Q_m = 3.0$ [m^3/s] is the suction discharge, and $\omega = 30$ [RPM] is the rotational speed of the cutter head, $V_{swing} = 0.2$ [m/s] is the swinging speed, the coordinate system is stream-wise and starting from the top of the breach face.

Table 2
Sand properties of the test case.

D_{30} (μm)	D_{50} (μm)	D_{60} (μm)	D_{90} (μm)	n_0	n_1	ϕ	ρs (kg/m^3)	k_l (m/s)
62.5	140	158	224	0.40	0.52	36	2650	3.07×10^{-3}

dynamic characteristics of the turbidity current, 3 values are tested for each parameter: a base value, a lower limit value (0.75 × the base value), and an upper limit value (1.25 × the base value). The other operational parameters are kept fixed while testing the concerned parameter. The upper and lower limits of the tested operational parameters are selected to be consistent with the operational ranges of the real-world cutter suction dredgers with a cutter head size similar to the tested one.

Figs. 12, 13 show the results of the turbidity current characteristics for the 3 tested scenarios of each operational parameter in addition to a case of considering breaching only. From these figures, we can notice an overall similar behaviour (trend) for U, C, and q along the 1-D domain; an increase along the breach face, a turning point at the end of the breach face (the point of bed slope transition), a rapid decrease within the first 10 m of the downstream part, and a gradual decrease for the remaining of the downstream part. This overall trend is governed by the breaching process along the breach face with its generated net-erosive turbidity current and the net-depositional behaviour of the turbidity current along the downstream part (see Figs. 12, and 13). The turning point at the end of the breach face is due to the transition from the net-erosive to the net-depositional flow regime. The rapid decrease within the first 10 m of the downstream part is due to the fast settling of the large sediment particles, which in turn rapidly decrease the concentration. Along the breach face, the sudden increase in the layer-averaged concentration (C) is due to the additional sediment source of the cutter head (mixing resuspension).

The impact of the operational parameters on the dynamics of the turbidity current (U, C, and q) is attributed to the contribution of each parameter to the mixing resuspension source. The cut ratio (Cut_{ratio}) has a dual impact, as it also contributes to the breaching resuspension source. In general, the mixing resuspension source increases with higher rotational speed (RPM), higher swinging speed (V_{swing}), and higher cut ratio (Cut_{ratio}) but with lower suction discharge ($Q_{suction}$). Conversely, decreasing RPM, V_{swing}, and Cut_{ratio} While increasing $Q_{suction}$ will result in a reduction in the mixing resuspension source. However, the degree of influence is different for each parameter.

Instead of assessing the relative importance of each parameter locally based on its 3 tested scenarios, a GSA is performed using the method of Sobol (1990). The sensitivity of the turbidity current characteristics to each operational parameter is quantified based on 10 240 samples (operational scenarios) with the variance-based total sensitivity Sobol index. To this end, the SALib Python library (Herman and Usher, 2017; Iwanaga et al., 2022) is used to perform the GSA. First, the 10 240 samples are generated using the sampling scheme of Saltelli (2002) included in the "sample" function within the SALIB library. The sampling scheme of Saltelli (2002) was proposed as an improvement of the Sobol sampling sequence (Sobol', 1967). Then, the developed model is automated to run the 10 240 operational scenarios and extract the turbidity current characteristics (U, C, and q) as the output parameters at the end of the modelled domain for each scenario. Finally, the Sobol total sensitivity index for each output parameter (U, C, and q) to each input parameter (RPM, V_{swing}, $Q_{suction}$, and Cut_{ratio}) is calculated using the "analyze" function within the SALIB library utilizing the values of the input and output parameters of the 12 040 sampled scenarios.

Fig. 14 shows the values and limits of the input parameters (RPM, V_{swing}, $Q_{suction}$, and Cut_{ratio}) and their corresponding output values (U, C, and q) for each sampled scenario. Fig. 15 shows the results of the total sensitivity index (ST) of the turbidity current characteristics (U, C, and q) to the operational parameters (RPM, V_{swing}, $Q_{suction}$, and Cut_{ratio}). These results show that the cut ratio (cut_{ratio}) is the most influential parameter on all turbidity current characteristics, with a value of about 0.8 for ST, representing the majority of the sensitivity scale (0–1). Away behind, $Q_{suction}$ comes second, and V_{swing} comes in the third place. The rotational speed (RPM) is the least significant parameter. The high

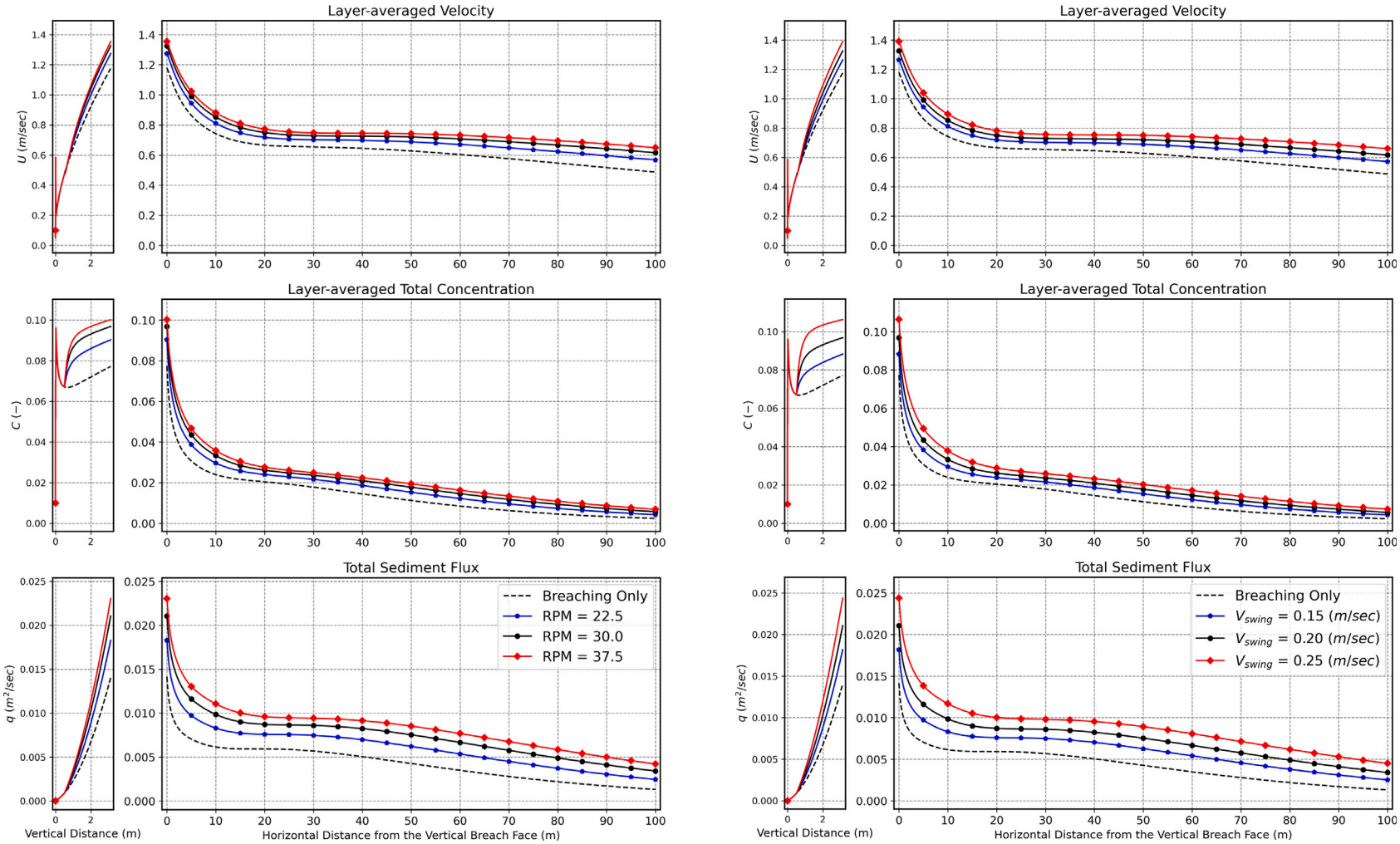

(a) Rotational speed (RPM)

(b) Swinging speed (V_{swing})

Fig. 12. Influence of the rotational speed and swinging speed on turbidity current characteristics. The black-dashed plot represents a case without cutter head mixing spillage (considering breaching only) and a breach height equal to the cutter head diameter ($Cut_{ratio} = 1.0$). The black-solid plot represents the reference case with rotational speed (RPM = 30), swinging speed ($V_{swing} = 0.2$ m/s), suction discharge ($Q_{suction} = 3.0$ m^3/s), and cut ratio ($Cut_{ratio} = 1.0$). The red plot represents the case of 25% increase of the concerned parameter (RPM or V_{swing}), and the blue blot represents the case of 25% decrease of the concerned parameter. The narrow plotting panels are for the breach face, while the wide plotting panels are for the downstream part.

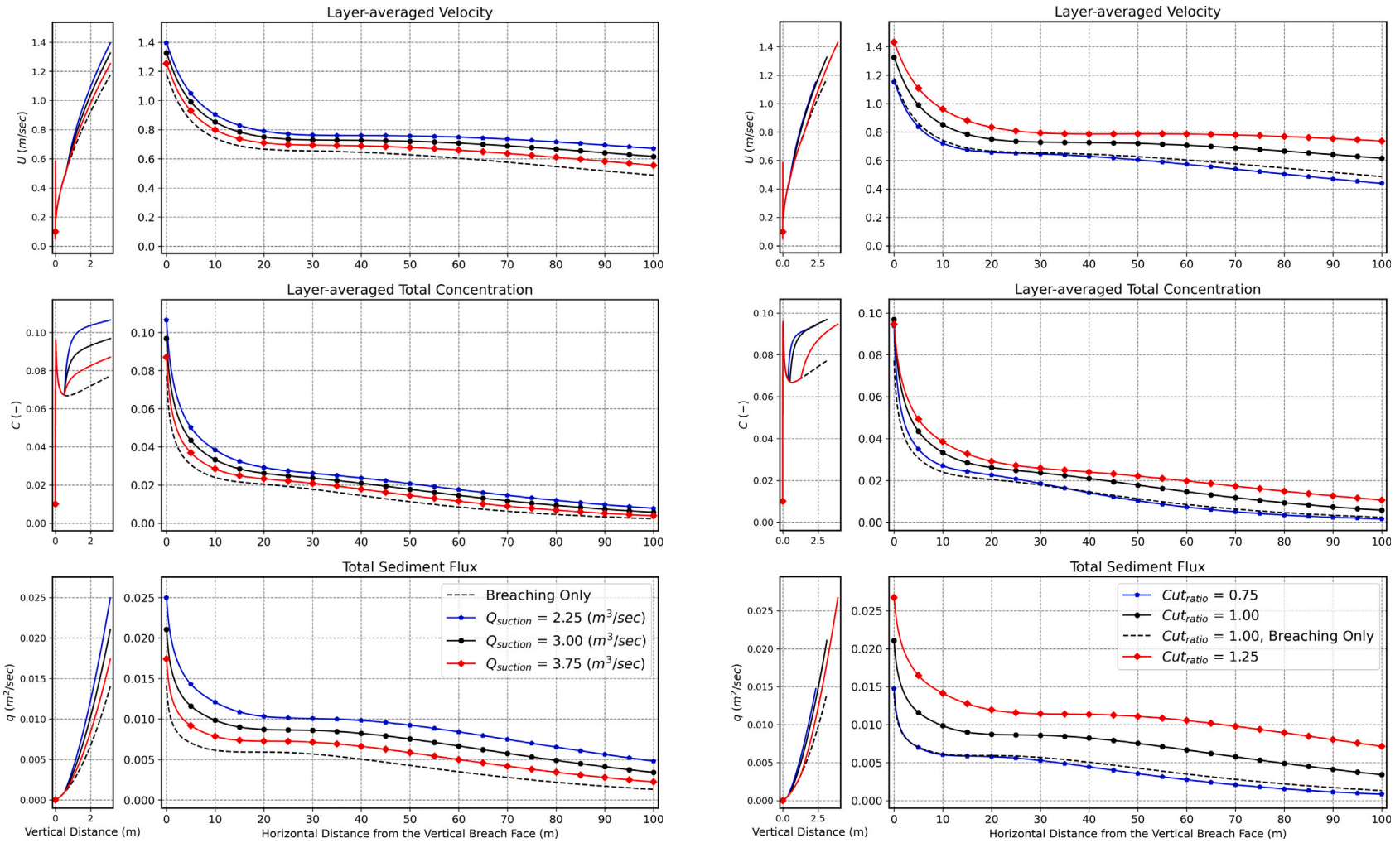

(a) Suction discharge ($Q_{suction}$) (b) Cut ratio (Cut_{ratio})

Fig. 13. Influence of the suction discharge and cut ratio on turbidity current characteristics, the black-dashed plot represents a case without cutter head mixing s (considering breaching only) and a breach height equal to the cutter head diameter (Cut_{ratio} = 1.0). The black-solid plot represents the reference case with rotational speed (RPM = 30), swinging speed (V_{swing} = 0.2 m/s), suction discharge ($Q_{suction}$ = 3.0 m^3/s), and cut ratio (Cut_{ratio} = 1.0). The red plot represents the case of 25% increase of the concerned parameter ($Q_{suction}$ or Cut_{ratio}), and the blue blot represents the case of 25% decrease of the concerned parameter. The narrow plotting panels are for the breach face, while the wide plotting panels are for the downstream part.

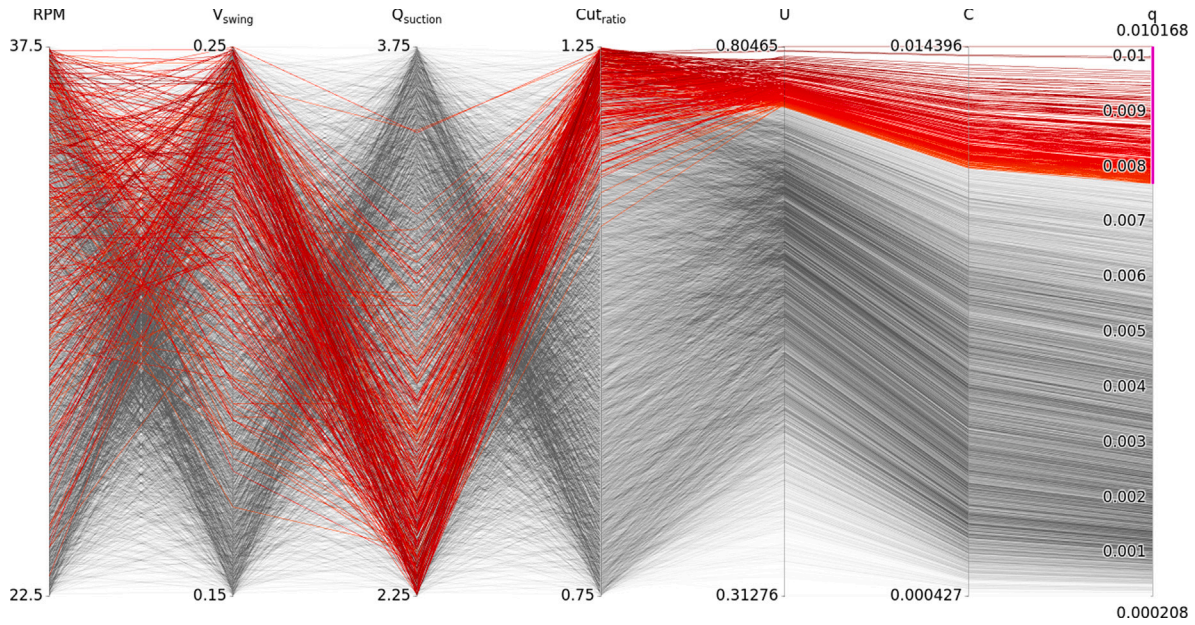

Fig. 14. Parallel plot of the 10 240 sampled operational scenarios. RPM, V_{swing} [m/s], $Q_{suction}$ [m^3/s], and Cut_{ratio} [−] are the input parameters, while the output parameters are the values of U [m/s], C [−], and q [m^2/s] at the end of the modelled domain. The red lines represent the 25% scenarios with the highest flux (q).

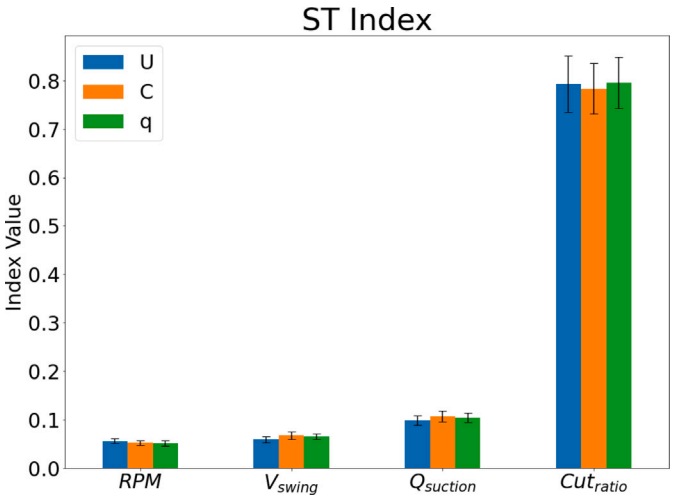

Fig. 15. Global sensitivity analysis results showing the total sensitivity index (ST) values for the tested operational parameters.

influence of the Cut_{ratio} can also be observed from its high correlation with the output parameters (U, C, and q) in Fig. 14; all the high values of U, C, and q stem from scenarios with high Cut_{ratio}.

7. Conclusions and outlook

This research was carried out to investigate the turbidity currents generated by cutter suction dredgers when dredging densely-packed sandy soils and to identify the relative influence of key operational parameters on these currents. To this end, a one-dimensional, steady-state, physics-based model was developed including two main resuspension mechanisms: breaching, and cutter head mixing spillage. The results showed that both breaching and mixing resuspension are major resuspension mechanisms. The breaching-related far-field sediment flux is not negligible compared to the far-field sediment flux related to the cutter head mixing spillage. Thus, breaching should be incorporated in the source-term estimation of cutter suction dredgers. Besides, the results of the global sensitivity analysis showed that the cut ratio (representing the cutting thickness) is the most influential parameter on turbidity. Such a finding can be utilized in the operation of cutter suction dredgers to reduce sediment release.

The model developed in this research has two main advantages; it is physics-based and computationally efficient, which makes it suitable for a variety of applications. It can be very helpful for qualitative assessment purposes to get insights into the order of magnitude of fluxes, concentration levels, and run-out distances of the CSD-induced turbidity currents for different operational scenarios and different in-situ bed properties. Besides, the model can also be used for operational management, sensitivity analysis, and optimization. It is worth noting that selecting the optimal operational parameters should be based on both dredging production and environmental constraints (e.g., suspended-sediment concentration). Once validated, the model can be considered as a base for a physics-based general approach for source-term estimations of cutter suction dredgers that can be extended to include other resuspension mechanisms and the dynamic interactions of the cutter head with the generated turbidity currents. To this end, in the future, we plan to conduct detailed laboratory experiments and computational fluid dynamics simulations to investigate the dynamic interaction of the cutter head with turbidity currents. This will allow for the validation of the present model and the assessment of the uncertainties arising from the simplifications made.

CRediT authorship contribution statement

Mosaab Mahgoub: Writing – original draft, Visualization, Methodology, Formal analysis, Data curation, Conceptualization. **G.H. Keetels:** Writing – original draft, Supervision, Methodology, Conceptualization. **Said Alhaddad:** Writing – review & editing, Writing – original draft, Visualization, Supervision, Project administration, Methodology, Conceptualization.

Declaration of competing interest

The authors declare that they have no known competing financial interests or personal relationships that could have appeared to influence the work reported in this paper.

References

Alhaddad, S., de Wit, L., Labeur, R.J., Uijttewaal, W., 2020a. Modeling of breaching-generated turbidity currents using large eddy simulation. J. Mar. Sci. Eng. 8 (9), 728.

Alhaddad, S., Elerian, M., 2024a. Mitigating suspended-sediment environmental pressure in subsea engineering through colliding turbidity currents. Res. Eng. 101916.

Alhaddad, S., Keetels, G., Mastbergen, D., van Rhee, C., Lee, C.-H., Montellà, E.P., Chauchat, J., 2024b. Subaqueous dilative slope failure (breaching): Current understanding and future prospects. Adv. Water Resour. 104708.

Alhaddad, S., Labeur, R.J., Uijttewaal, W., 2020b. Breaching flow slides and the associated turbidity current. J. Mar. Sci. Eng. 8 (2), 67.

Alhaddad, S., Labeur, R.J., Uijttewaal, W., 2020c. Large-scale experiments on breaching flow slides and the associated turbidity current. J. Geophys. Res.: Earth Surf. 125 (10), e2020JF005582. http://dx.doi.org/10.1029/2020JF005582.

Alhaddad, S., Labeur, R., Uijttewaal, W., 2021. Preliminary evaluation of existing breaching erosion models. In: 10th International Conference on Scour and Erosion. ISSMGE, pp. 619–627.

Alhaddad, S., Weij, D., van Rhee, C., Keetels, G., 2023. Stabilizing and destabilizing breaching flow slides. J. Mar. Sci. Eng. 11 (3), 560.

Archer, G.E.B., Saltelli, A., Sobol, I.M., 1997. Sensitivity measures,anova-like techniques and the use of bootstrap. J. Stat. Comput. Simul. 58 (2), 99–120. http://dx.doi.org/10.1080/00949659708811825.

Becker, J., 2011. Dredge Plumes: Ecological Risk Assessment. Delft University of Technology.

Becker, J., van Eekelen, E., van Wiechen, J., de Lange, W., Damsma, T., Smolders, T., van Koningsveld, M., 2015. Estimating source terms for far field dredge plume modelling. J. Environ. Manage. 149, 282–293.

Borgonovo, E., Plischke, E., 2016. Sensitivity analysis: A review of recent advances. European J. Oper. Res. 248 (3), 869–887. http://dx.doi.org/10.1016/j.ejor.2015.06.032, URL https://www.sciencedirect.com/science/article/pii/S0377221715005469.

Brandstäter, S., 2021. Global Sensitivity Analysis for Models of Active Biomechanical Systems (Ph.D. thesis). Technische Universität München.

Breusers, H., 1977. Hydraulic excavation of sand. In: Proceedings International Course in Modern dreding.

Brownlie, W.R., 1982. Prediction of flow depth and sediment discharge in open channels (Ph.D. thesis). California Institute of Technology Pasadena, CA.

Collins, M.A., 1995. Dredging-Induced Near-Field Resuspended Sediment Concentrations and Source Strengths. Vol. 95, US Army Engineer Waterways Experiment Station.

Crockett, T.R., 1993. Modelling Near Field Sediment Resuspension in Cutterhead Suction Dredging Operations. University of Nebraska-Lincoln.

De Wit, L., 2015. 3D CFD modelling of overflow dredging plumes (Ph.D. thesis). Delft University of Technology.

Den Burger, M., 2003. Mixture Forming Processes in Dredge Cutter Heads (Ph.D. thesis). Delft University of Technology.

Eke, E., Viparelli, E., Parker, G., 2011. Field-scale numerical modeling of breaching as a mechanism for generating continuous turbidity currents. Geosphere 7 (5), 1063–1076.

EPA, 2021. Technical guidance: Environmental impact assessment of marine dredging proposals. Environ. Prot. Auth. Perth West. Aust..

Erftemeijer, P.L., Riegl, B., Hoeksema, B.W., Todd, P.A., 2012. Environmental impacts of dredging and other sediment disturbances on corals: a review. Mar. Pollut. Bull. 64 (9), 1737–1765.

Erftemeijer, P.L., Robin Lewis, R.R., 2006. Environmental impacts of dredging on seagrasses: a review. Mar. Pollut. Bull. 52 (12), 1553–1572.

Ferguson, R., Church, M., 2004. A simple universal equation for grain settling velocity. J. Sediment. Res. 74 (6), 933–937.

Fukushima, Y., Parker, G., Pantin, H., 1985. Prediction of ignitive turbidity currents in scripps submarine canyon. Mar. Geol. 67 (1–2), 55–81.

Garcia, M., Parker, G., 1993. Experiments on the entrainment of sediment into suspension by a dense bottom current. J. Geophys. Res.: Oceans 98 (C3), 4793–4807.

Groenenberg, R.M., Sloff, K., Weltje, G.J., 2009. A high-resolution 2-DH numerical scheme for process-based modeling of 3-D turbidite fan stratigraphy. Comput. Geosci. 35 (8), 1686–1700.

Hayes, D.F., 1986. Development of a Near Field Source Strength Model to Predict Sediment Resuspension from Cutter Suction Dredges. Mississippi State University.

Hayes, D.F., Crockett, T.R., Ward, T.J., Averett, D., 2000. Sediment resuspension during cutterhead dredging operations. J. Waterw. Port Coast. Ocean Eng. 126 (3), 153–161.

Hayes, D., Wu, P.-Y., 2001. Simple approach to TSS source strength estimates. In: Proceedings of the WEDA XXI Conference, Houston, TX, June 25. Vol. 27, p. 2001.

Henriksen, J.C., 2009. Near-Field Sediment Resuspension Measurement and Modeling for Cutter Suction Dredging Operations (Ph.D. thesis). Texas A&M University.

Herman, J., Usher, W., 2017. SALib: An open-source python library for sensitivity analysis. J. Open Sour. Softw. 2 (9), http://dx.doi.org/10.21105/joss.00097.

HR Wallingford, 2003. Protocol for the Field Measurement of Sediment Release from Dredgers. HR Wallingford Ltd. & Dredging Research Ltd..

Hu, P., Pähtz, T., He, Z., 2015. Is it appropriate to model turbidity currents with the three-equation model? J. Geophys. Res.: Earth Surf. 120 (7), 1153–1170. http://dx.doi.org/10.1002/2015JF003474.

Iooss, B., Lemaître, P., 2015. A review on global sensitivity analysis methods. Uncertainty Management in Simulation-Optimization of Complex Systems: Algorithms and Applications. Springer, pp. 101–122.

Iwanaga, T., Usher, W., Herman, J., 2022. Toward SALib 2.0: Advancing the accessibility and interpretability of global sensitivity analyses. Socio-Environ. Syst. Model. 4, 18155. http://dx.doi.org/10.18174/sesmo.18155, URL https://sesmo.org/article/view/18155.

Jones, R., Fisher, R., Bessell-Browne, P., 2019. Sediment deposition and coral smothering. PLoS One 14 (6), e0216248.

Karassik, I.J., Messina, J.P., Cooper, P., Heald, C.C. (Eds.), 2008. Pump Handbook, fourth ed. McGraw-Hill Education, New York.

Kostic, S., Parker, G., 2006. The response of turbidity currents to a canyon–fan transition: internal hydraulic jumps and depositional signatures. J. Hydraul. Res. 44 (5), 631–653.

Louis, A., 2017. On Creating a Numerical Model for Estimating Spillage in a Cutter Suction Dredger While Cutting Sand. Delft University of Technology.

Miedema, S.A., 2019. Dredging Engineering: Special Topics. TU Delft Open.

Miedema, S., Nieuwboer, B., 2019. Cutter head spillage when dredging sand or gravel. In: Hayes, D. (Ed.), Proceedings of the Dredging Summit and Expo 2019. Western Dredging Association, pp. 247–266.

Mills, D., Kemps, H., 2016. Generation and release of sediments by hydraulic dredging: a review. Rep. Theme 2.

Niewboer, B., 2022. Modelling Spillage in Rotating Cutter Suction Heads: A Combined Finite Volume and Discrete Element Model (Ph.D. thesis). Delft University of Technology.

Parker, G., 1982. Conditions for the ignition of catastrophically erosive turbidity currents. Mar. Geol. 46 (3–4), 307–327.

Parker, G., Fukushima, Y., Pantin, H.M., 1986. Self-accelerating turbidity currents. J. Fluid Mech. 171, 145–181.

Parker, G., Garcia, M., Fukushima, Y., Yu, W., 1987. Experiments on turbidity currents over an erodible bed. J. Hydraul. Res. 25 (1), 123–147.

PIANC, 2010. Dredging and Port Construction Around Coral Reefs. PIANC Secretariat.

Pianosi, F., Beven, K., Freer, J., Hall, J.W., Rougier, J., Stephenson, D.B., Wagener, T., 2016. Sensitivity analysis of environmental models: A systematic review with practical workflow. Environ. Model. Softw. 79, 214–232.

Richardson, J., Zaki, W., 1954. The sedimentation of a suspension of uniform spheres under conditions of viscous flow. Chem. Eng. Sci. 3 (2), 65–73.

Saltelli, A., 2002. Making best use of model evaluations to compute sensitivity indices. Comput. Phys. Commun. 145 (2), 280–297.

Saltelli, A., Aleksankina, K., Becker, W., Fennell, P., Ferretti, F., Holst, N., Li, S., Wu, Q., 2019. Why so many published sensitivity analyses are false: A systematic review of sensitivity analysis practices. Environ. Model. Softw. 114, 29–39.

Saltelli, A., Ratto, M., Andres, T., Campolongo, F., Cariboni, J., Gatelli, D., Saisana, M., Tarantola, S., 2008. Global Sensitivity Analysis: The Primer. John Wiley & Sons.

Shao, D., Purnama, A., Sun, T., 2015. Modeling the temporal evolution of dredging-induced turbidity in the far field. J. Waterw. Port Coast. Ocean Eng. 141 (5), 04015001.

Sobol', I., 1967. On the distribution of points in a cube and the approximate evaluation of integrals. USSR Comput. Math. Math. Phys. 7 (4), 86–112. http://dx.doi.org/10.1016/0041-5553(67)90144-9, URL https://www.sciencedirect.com/science/article/pii/0041555367901449.

Sobol, I., 1990. On sensitivity estimation for nonlinear mathematical models. Mat. Model. 2 (1), 112–118.

Sobol, I.M., 2001. Global sensitivity indices for nonlinear mathematical models and their Monte Carlo estimates. Math. Comput. Simul. 55 (1–3), 271–280.

Sun, C., Branson, P.M., Mills, D., 2020. Guideline on dredge plume modelling for environmental impact assessment.

Tuinhof, T., 2014. Modelling Far-Field Dredge Plume Dispersion. Delft University of Technology.

Vlasblom, W., 2005. The Cutter Suction Dredger. Delft University of Technology, Delft, Nehterlands.

Werkhoven, J., 2019. CSD Spillage Model for Sand and Rock: A Particle Size-Agnostic, Adaptable Engineering Model for the Prediction of Cutter Suction Dredge Spillage Rates. Delft University of Technology.

Werkhoven, J.J., Nieuwboer, B.J., Louis, A.A., Ramsdell, R.C., Miedema, S.A., 2018. A pseudo-analytical model CSD spillage due to rotational velocity-induced flow. In: Proceedings of the Western Dredging Association Dredging Summit & Expo'18. pp. 25–28.